

VerSe: Integrating Multiple Queries as Prompts for Versatile Cardiac MRI Segmentation

Bangwei Guo¹, Meng Ye¹, Yunhe Gao¹, Bingyu Xin¹, Leon Axel², and Dimitris Metaxas¹

¹ Rutgers University

² New York University School of Medicine

Abstract. Despite the advances in learning-based image segmentation approach, the accurate segmentation of cardiac structures from magnetic resonance imaging (MRI) remains a critical challenge. While existing automatic segmentation methods have shown promise, they still require extensive manual corrections of the segmentation results by human experts, particularly in complex regions such as the basal and apical parts of the heart. Recent efforts have been made on developing interactive image segmentation methods that enable human-in-the-loop learning. However, they are semi-automatic and inefficient, due to their reliance on click-based prompts, especially for 3D cardiac MRI volumes. To address these limitations, we propose **VerSe**, a **Versatile Segmentation** framework to unify automatic and interactive segmentation through multiple queries. Our key innovation lies in the joint learning of object and click queries as prompts for a shared segmentation backbone. **VerSe** supports both fully automatic segmentation, through object queries, and interactive mask refinement, by providing click queries when needed. With the proposed integrated prompting scheme, **VerSe** demonstrates significant improvement in performance and efficiency over existing methods, on both cardiac MRI and out-of-distribution medical imaging datasets. The code is available at <https://github.com/bangwayne/Verse>.

Keywords: Cardiac MRI · Multiple Prompts · Versatile Segmentation.

1 Introduction

Cardiac magnetic resonance imaging (MRI) can provide comprehensive information for heart disease diagnosis and treatment [31], serving as the gold standard for various clinical applications. For example, cardiac cine MRI [3] enables precise evaluation of cardiac function, while cardiac late gadolinium enhancement (LGE) MRI [33] excels in detecting myocardium infarction (MI) and assessing tissue viability. Despite these advantages, the widespread clinical adoption of cardiac MRI lags behind echo cardiography and computational tomography (CT), in large part due to the challenges in image post-processing, *e.g.*, the accurate segmentation of anatomical structures and lesions.

Deep learning-based methods have significantly improved automatic cardiac MRI segmentation. U-Net [34] and its variants [16,18,30] remain the most widely

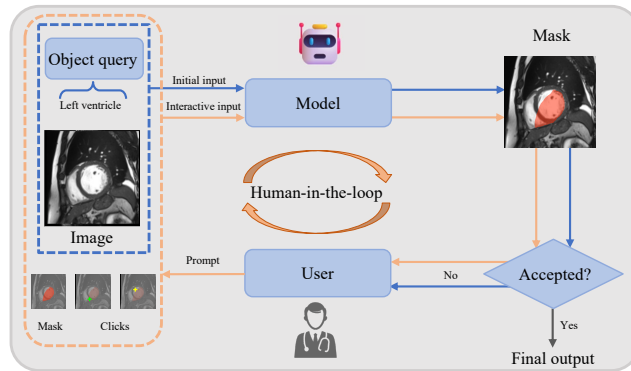


Fig. 1. Illustration of the proposed versatile segmentation framework. Our model accepts an object query, such as left ventricle, to automatically segment the target in the image. If the initial segmentation is unsatisfactory, users can refine the mask by providing corrective clicks until the final output mask can meet clinical accuracy.

used architecture and perform well on both 2D and 3D images, but struggle with intricate object boundaries and complex structures [4]. Vision Transformer (ViT)-based models [8,13,38] effectively capture long-range dependencies but demand extensive datasets for optimal performance. Hybrid models, like UT-Net [16] and MedFormer [15] enhance segmentation performance by combining convolutional neural networks (CNNs) and transformers. Despite these advances, current methods still fail to meet clinical precision requirements, particularly in challenging basal and apical regions [5]. These limitations often necessitate time-consuming manual corrections by experts, highlighting the gap between automated methods and clinical precision, especially for large-scale applications.

To address the limitations of fully automatic segmentation approaches, interactive image segmentation methods have been proposed to facilitate efficient segmentation and annotation [28,35,36]. These methods commonly rely on user clicks to guide learning-based models, mimicking human corrections and significantly improving efficiency compared to traditional pixel-by-pixel annotations. Early work [36] first introduced CNN-based interactive segmentation, while RITM [35] enhanced it by integrating mask information from previous iterations. Recently, ViT-based models like SimpleClick [28] and SegNext [27] have achieved state-of-the-art performance by leveraging large-scale ViT architectures and extensive pretraining on natural image datasets. However, these advancements rely heavily on advanced backbones and high-quality data, while their use of point-based prompts remains rudimentary. Notably, no interactive segmentation models have been tailored for cardiac MRIs, despite its pressing clinical demand and heavy reliance on user inputs. This gap highlights the urgent need for more efficient interactive segmentation solutions.

Recent advances in universal image segmentation [9,14] have explored efficient designs that combine learnable queries [12,25,37] with transformer de-

coders [7]. These works have inspired us to propose a novel image segmentation paradigm that leverages both data priors and human expert intelligence. As illustrated in Fig. 1, we introduce **VerSe**, a **Versatile cardiac MRI Segmentation** model that integrates automatic and interactive segmentation into a unified framework. Central to our approach is the introduction of multi-query integration, which serves as prompts for a shared segmentation backbone. This design enables our model to operate seamlessly across multiple modes, enhancing its flexibility and adaptability to diverse segmentation tasks.

Our contributions are summarized as follows: (1) We introduce a novel cardiac MRI segmentation paradigm that unifies automatic and interactive segmentation, bridging the gap between learning-based methods and large-scale clinical usage through the fusion of machine and human intelligence. (2) We propose a new image segmentation architecture which can integrate multiply queries, *i.e.*, object query and click query, to prompt a foundational segmentation backbone. (3) We conducted extensive experiments on seven cardiac MRI datasets. The results demonstrate the high accuracy, efficiency, and versatility of our segmentation model. Our method also shows the potential for generalization to other out-of-distribution medical imaging segmentation tasks.

2 Method

2.1 Overview

We propose a novel **Versatile image Segmentation** model, **VerSe**, through the integration of object query and click query. An overview of **VerSe** architecture is shown in Fig. 2. In the following, we give details of the proposed method.

2.2 Multi-Query Integration as Prompt

To enable multiple functions within our model, we introduce the **Multi-Query Integration** mechanism, which guides the model to focus on relevant objects. For the automatic segmentation task, instead of using CLIP-based semantic embeddings [26], we employ learnable object queries \mathbf{X}_o , as they provide stronger task-specific prior knowledge [14]. Each segmentation target is represented by a small group of learnable query vectors. Specifically, for N target objects, we assign N groups of learnable queries $\mathbf{X}_o = [\mathbf{X}_{o1}, \dots, \mathbf{X}_{oi}, \dots, \mathbf{X}_{oN}]$, where each group $\mathbf{X}_{oi} \in \mathbb{R}^{M \times C}$ consists of M query vectors with C channels. These queries are initialized as random parameters and optimized during training.

For the interactive segmentation task based on clicks, inspired by SAM [19], we encode the click locations as sparse positional queries \mathbf{X}_s . For a positive click set $\mathcal{C}_p = \{(x_1, y_1), \dots, (x_{N_p}, y_{N_p})\}$, we use a Point Encoder to encode each click point to a corresponding positive positional query \mathbf{X}_{sp} , generating $N_p \times C$ vectors. The same process applies for the negative click set \mathcal{C}_n and the corresponding negative positional queries are denoted as \mathbf{X}_{sn} .

To further enhance the effectiveness of click prompts, we propose a novel **Semantic Feature Query** \mathbf{X}_f , as illustrated in Fig. 3(a). The image encoder

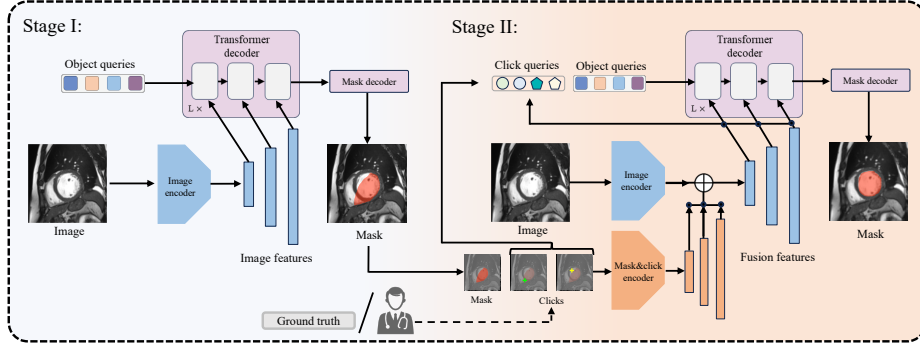


Fig. 2. Overview of the **VerSe** architecture. In stage I, object queries are used to automatically segment a target in the image. In stage II, user provides clicks as prompts to refine the initial segmentation mask. **VerSe** also supports a pure interactive mode, where the initial mask is empty and the object queries aren’t activated. The image encoder, transformer decoder and mask decoder are shared across all stages. Implementation details are described in Sec. 2.5.

extracts multiple down-scaling features from the input image. For a feature map \mathbf{F}_s with shape $(H/s, W/s)$, where s is the down-scaling factor and H, W are the original image height and width, we first map the original click point $P_0 = (x, y)$ to its corresponding coordinates in the down-scaling feature map $P'_0 = (x', y')$:

$$x' = \lfloor \frac{x}{s} \rfloor, \quad y' = \lfloor \frac{y}{s} \rfloor. \quad (1)$$

We then extract features from a $(2r+1) \times (2r+1)$ window around P'_0 and apply average pooling to compute $\mathbf{f}_{\text{pooled}}$:

$$\mathbf{f}_{\text{pooled}} = \frac{1}{(2r+1)^2} \sum_{i=-r}^r \sum_{j=-r}^r \mathbf{F}_s(x'+i, y'+j). \quad (2)$$

Finally, $\mathbf{f}_{\text{pooled}}$ is projected into a new feature space via a multilayer perceptron (MLP):

$$\mathbf{X}_{f_0} = \text{MLP}(\mathbf{f}_{\text{pooled}}), \quad (3)$$

where $\mathbf{X}_{f_0} \in \mathbb{R}^{1 \times C}$ represents the semantic feature query for the click at P_0 . Positive and negative click sets generate semantic feature queries \mathbf{X}_{fp} and \mathbf{X}_{fn} , respectively, at three feature scales $s = 2, 4, 8$.

\mathbf{X}_o , \mathbf{X}_s , and \mathbf{X}_f collaboratively enable the versatile functions of our model. Specifically, click queries \mathbf{X}_c are formed by combining sparse positional queries \mathbf{X}_s and semantic feature queries \mathbf{X}_f . Leveraging multi-query integration, **VerSe** flexibly supports three working modes:

- **Mode-1:** Automatic segmentation directed by object queries \mathbf{X}_o ;
- **Mode-2:** Interactive refinement of the initial segmentation from Mode-1 by combining object queries \mathbf{X}_o and click queries \mathbf{X}_c ;

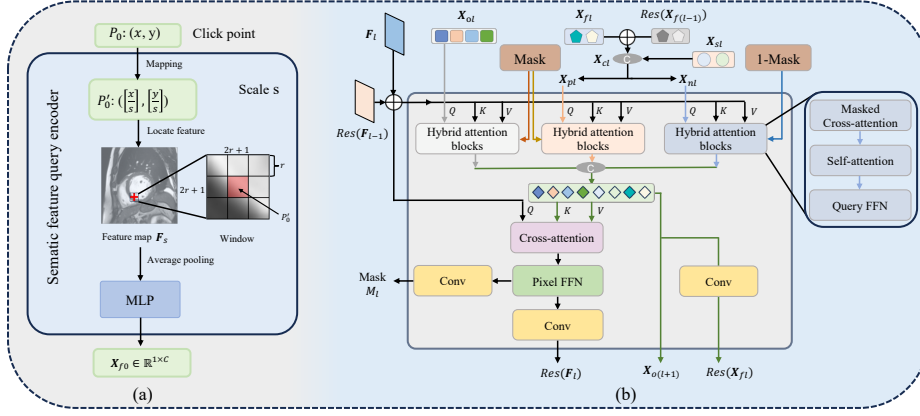


Fig. 3. (a) Process of generating semantic feature query X_{f0} for a specified click point P_0 at scale s . The original click P_0 is mapped to the coordinates P'_0 on the down-scaling feature map. A feature patch centered at P'_0 undergoes average pooling, and the resulting feature is transformed via an MLP to produce X_{f0} . (b) Transformer decoder at the l -th layer. Object queries X_{ol} , positive click queries X_{pl} and negative click queries X_{nl} first interact with image features F_l , to capture foreground target and background context. These queries are then concatenated to update the image features. X_{fl} , X_{sl} , and X_{cl} denote semantic feature queries, sparse positional queries, and click queries at the l -th layer, respectively.

- **Mode-3:** Purely interactive segmentation guided by user clicks, relying solely on click queries X_c .

2.3 Foreground-Background Masked Attention

After obtaining all queries, we update the image features by attending to the multiple queries. As shown in Fig. 3(b), we use foreground-background masked attention [9,10] to guide multiple queries in focusing on the target-related image features, as well as gathering background information. Unlike [10], we explicitly separate the foreground target from the background using foreground and background click prompts. Specifically, we define positive click queries $X_p = \{X_{sp}, X_{fp}\}$ and negative click queries $X_n = \{X_{sn}, X_{fn}\}$. To ensure X_p and X_n have the same size of $N_1 \times C$, we add dummy points to pad X_p and X_n when click number is smaller than N_1 . In our implementation, we set $N_1 = 24$. Our foreground-background masked cross-attention is computed as:

$$X'_{ol} = \text{softmax}(M_{pl} + Q_{ol}K_l^T)V_l + X_{ol}, \quad (4)$$

$$X'_{pl} = \text{softmax}(M_{pl} + Q_{pl}K_l^T)V_l + X_{pl}, \quad (5)$$

$$X'_{nl} = \text{softmax}(M_{nl} + Q_{nl}K_l^T)V_l + X_{nl}, \quad (6)$$

where l is the layer index of the transformer decoder shown in Fig. 2 and Fig. 3(b). \mathbf{Q}_{*l} is the learned linear transformation of \mathbf{X}_{*l} , where $*$ denotes different query types, *i.e.*, object, positive and negative click queries. $\mathbf{K}_l, \mathbf{V}_l$ are the learned linear transformations of image features \mathbf{F}_l . $\mathbf{M}_{pl}, \mathbf{M}_{nl} \in \{0, -\infty\}^{N_1 \times H_l W_l}$ are used to control the foreground-background attention masking. At the l -th layer, we first generate a mask prediction \mathbf{M}_l from the pixel features \mathbf{F}_{l-1} of the previous $(l-1)$ -th layer, using a simple mask decoder followed by proper mask resizing. Then, \mathbf{M}_{pl} and \mathbf{M}_{nl} at feature location (x, y) are calculated as:

$$\mathbf{M}_{pl}(x, y) = \begin{cases} 0, & \mathbf{M}_l(x, y) \geq 0.5 \\ -\infty, & \text{otherwise} \end{cases}, \quad \mathbf{M}_{nl}(x, y) = \begin{cases} 0, & \mathbf{M}_l(x, y) < 0.5 \\ -\infty, & \text{otherwise} \end{cases}. \quad (7)$$

Next, $\mathbf{X}'_{ol}, \mathbf{X}'_{pl}, \mathbf{X}'_{nl}$ are processed separately through self-attention and query feedforward networks (FFN). The resulting queries are concatenated along the query number dimension, then transformed into the **Key** and **Value** spaces using learned linear transformations. A cross-attention layer, with image features as the **Query**, followed by a pixel FFN, updates the image features, which are finally used to generate the segmentation mask.

2.4 Residual Connection with Different Scales

In our multi-scale transformer decoder, the integrated queries forward through different decoder layers, continuously interacting with image features across scales. To enhance the interaction between image features and integrated queries across various scales, we adopt a residual [17] resampling connection similar to the U-Net [34] decoder. For the image feature map \mathbf{F}_l at layer l , it's first resampled to align with the resolution of \mathbf{F}_{l+1} at next layer $l+1$:

$$\mathbf{F}_l^{\text{resampled}} = \text{Resample}(\mathbf{F}_l, \text{size}(\mathbf{F}_{l+1})). \quad (8)$$

Here, $\text{Resample}(\cdot)$ can involve upsampling or downsampling depending on the change in scale. Next, we apply a convolutional layer to calculate the residual $\text{Res}(\mathbf{F}_l)$ before adding it to the feature at the next layer. The updated feature map at scale $l+1$ is computed as:

$$\mathbf{F}_{l+1}^{\text{updated}} = \mathbf{F}_{l+1} + \text{Res}(\mathbf{F}_l) = \mathbf{F}_{l+1} + \text{Conv}(\mathbf{F}_l^{\text{resampled}}). \quad (9)$$

A similar operation is applied to semantic feature queries \mathbf{X}_f . By iteratively resampling, computing residuals, and updating features at each scale, the model effectively integrates multi-scale context, enhancing the interaction between features and queries across scales.

2.5 Implementation Details

Image Encoder. We utilize UTMNet [16] as the image encoder, which is specifically designed for cardiac MRI segmentation. We extract multi-scale features at

resolutions of 1/8, 1/4, and 1/2 of the original image, providing a comprehensive feature representation across different scales ($S = 3$).

Mask&Click Encoder. We use simple consecutive convolutional layers to encode the dense mask&click feature map. Starting with original dimensions of $(3, H, W)$, the layers downsample it to 1/8, 1/4, and 1/2 of the original size, matching the feature scales of the image encoder for seamless feature addition.

Click Representation. During training and inference, clicks are represented as disk maps with a fixed radius of 1. Following prior work [28,35], clicks are simulated by comparing current segmentation with ground truth. Unlike RITM [35], we place new clicks at the center of the largest connected component in misclassified regions, better aligning with user interactions in medical imaging. In Mode-1 and Mode-2, the model generates an initial mask, using object queries, and refines it with 2 clicks. In Mode-3, it iteratively uses 3 clicks without object queries to produce 3 segmentation masks.

Transformer Decoder. We use our transformer decoders proposed in Sec. 2 with $L = 2$ (*i.e.*, 6 layers in total). Similar to [9], we use a round robin approach for $L \times$ multi-scale interaction between image features and integrated queries.

Training Settings and Strategy. Our models are trained for 75 epochs with a batch size of 8 on 8 Quadro RTX 8000 GPUs. Images are resized to 256×256 during both training and inference. We use a combination of binary cross-entropy loss and Dice loss [30] to compute the mask loss $\mathcal{L} = \lambda_{ce}\mathcal{L}_{ce} + \lambda_{dice}\mathcal{L}_{dice}$, where $\lambda_{ce} = \lambda_{dice} = 5.0$. To enhance model robustness, we employ the following data augmentation techniques: 1) Random flips along both horizontal and vertical axes, 2) Random 90-degree rotations, 3) Random adjustments to brightness, and 4) Random adjustments to contrast. To support the diverse working modes of **Verse** during evaluation, we adopt a random training strategy. More specifically, each training batch is randomly assigned to Mode-1&2 or Mode-3.

3 Experiments

Datasets. We conducted experiments on nine publicly available datasets, including seven cardiac MRI datasets and two out-of-distribution medical imaging datasets, as summarized in Table 1. While 3D image volumes are provided in these datasets, we performed all experiments on 2D image slices, excluding slices without any instances. Our combined cardiac training set includes three types of cardiac MRI data: (1) **Balanced Steady-State Free Precession (bSSFP)** sequences, which focus on segmenting the left ventricle (LV), right ventricle (RV), and myocardium wall (Myo); (2) **T2-weighted (T2)** sequences, which highlight myocardial edema; and (3) **LGE** sequences, which highlight myocardial scar. For the M&Ms-2 dataset, we utilized only long-axis (LA) cine MRI images, to enhance data diversity, while other bSSFP datasets were acquired as short-axis images. For out-of-distribution evaluation, we tested our method on OAIZIB [1], a knee MRI dataset acquired with **Double Echo Steady State (DESS)** sequence, and BraTS [2], a brain **T2-weighted** MRI dataset. These datasets allow us to assess the generalizability of our model to different domains.

Table 1. Datasets statistics. The upper cardiac MRI datasets are for upstream training and analysis. The bottom two out-of-distribution datasets are for downstream tasks on assessing generalizability of interactive segmentation models.

Dataset	Targets	Modality	3D Volumes		2D Slices	
			Train	Test	Train	Test
ACDC [4]	LV, Myo, RV	bSSFP	200	100	1841	1001
M&Ms [5]	LV, Myo, RV	bSSFP	300	340	2475	2821
M&Ms-2 [5]	LV, Myo, RV	bSSFP	400	320	400	320
MyoPS++ [11,20,32,39]	LV, Myo, RV	bSSFP	90	29	672	194
MyoPS++ [11,20,32,39]	Myocardial Edema	T2	38	12	231	79
MyoPS++ [11,20,32,39]	Myocardial Scar	LGE	56	18	313	98
LASCARQS++ [21,22,23,24]	Left Atrial	LGE	98	32	3561	1183
OAIZIB [1]	Knee Bone&Cartilage	DESS	-	-	-	150
BraTS [2]	Brain Tumor	T2	-	-	-	369

Baseline Methods. For automatic image segmentation, we compared our method with nnU-Net [18], TransUNet [8], UTNet [16], Swin-UNet [6] and MedFormer [15], all of which are widely recognized and applied in medical image segmentation. For interactive image segmentation, we compared our method with RITM [35], iSegformer [29], SimpleClick [28] and SegNext [27]. Among these, SimpleClick and SegNext are the state-of-the-art (SOTA) methods for interactive segmentation, demonstrating exceptional performance across various benchmarks.

Evaluation Metrics. We use the 2D Dice score to evaluate the segmentation accuracy, which is a standard measure in medical image segmentation [4,16]. We use the Number of Clicks (NoC) metric to assess the number of clicks required to reach a specified Dice score. Target Dice scores are set at 80%, 85%, 90%, and 95%, denoted as Noc80, NoC85, NoC90, and NoC95, respectively. Each instance allows a maximum of 20 clicks. In addition, we evaluated segmentation quality using the average Dice score of all instances at a fixed number of clicks, $Dice(n)$.

3.1 Results

Comparison with Automatic Models. Table 2 compares our proposed VerSe framework with several specialized segmentation models designed for specific tasks. Despite lacking any specialized design to enhance automatic segmentation, VerSe achieves competitive performance on large-scale datasets such as ACDC and M&Ms, demonstrating its robustness and adaptability across diverse segmentation scenarios. However, on more challenging datasets like MyoPS++ (T2), where all models struggle to meet clinical requirements, due to the dataset’s inherent complexity, the interactive capabilities of VerSe become particularly advantageous. By enabling efficient user-driven refinements through click-based interactions, VerSe provides a practical solution to enhance segmentation accuracy in challenging cases, bridging the gap toward clinical applicability.

Comparison with Interactive Models. Table 2 highlights the performance comparison between VerSe (Mode-3) and previous SOTA interactive models.

Table 2. Model performance comparison for different working mode settings and different cardiac MRI datasets. Our method is the only one that can work in both automatic and interactive image segmentation modes.

Dataset	Automatic		Interactive					
	Model	Dice \uparrow	Model	Dice(1) \uparrow	Dice(20) \uparrow	NoC85 \downarrow	NoC90 \downarrow	NoC95 \downarrow
ACDC (bSSFP)	nnUNet	89.796	RITM	83.999	92.911	2.175	4.784	11.055
	TranUNet	87.649	iSegformer	66.595	92.498	4.251	7.371	12.384
	UTNet	89.604	SimpleClick	88.050	92.293	2.402	5.468	11.647
	SwinUNet	87.883	SegNext	87.665	92.265	2.295	5.397	11.794
	Medformer	86.931	VerSe (Mode-3)	89.757	96.698	1.485	2.352	6.480
	VerSe (Mode-1)	89.788	VerSe (Mode-2)	92.091	96.865	0.431	1.248	5.636
M&Ms (bSSFP)	nnUNet	85.417	RITM	80.583	92.855	2.709	5.772	12.146
	TranUNet	85.212	iSegformer	62.285	91.635	4.947	8.161	13.418
	UTNet	85.998	SimpleClick	85.335	91.289	3.787	6.809	13.216
	SwinUNet	84.363	SegNext	85.197	91.676	3.375	6.502	13.209
	Medformer	84.472	VerSe (Mode-3)	87.460	96.827	1.968	3.074	6.828
	VerSe (Mode-1)	86.527	VerSe (Mode-2)	89.429	96.887	1.013	2.122	5.906
M&Ms-2 (bSSFP)	nnUNet	90.638	RITM	85.829	93.606	3.214	6.082	10.474
	TranUNet	89.543	iSegformer	58.925	92.860	6.828	9.066	12.430
	UTNet	90.266	SimpleClick	88.880	93.951	2.004	4.376	9.619
	SwinUNet	89.098	SegNext	87.907	93.599	2.196	5.050	10.366
	Medformer	87.544	VerSe (Mode-3)	88.357	97.057	1.800	3.015	7.671
	VerSe (Mode-1)	86.496	VerSe (Mode-2)	89.830	97.013	0.884	2.194	7.047
MyoPS++ (bSSFP)	nnUNet	88.316	RITM	84.800	92.694	2.311	5.807	12.635
	TranUNet	86.886	iSegformer	66.061	92.282	5.619	8.951	13.488
	UTNet	87.583	SimpleClick	88.030	92.279	1.868	4.777	12.184
	SwinUNet	86.743	SegNext	86.431	92.422	2.189	5.502	12.551
	Medformer	87.417	VerSe (Mode-3)	88.834	97.079	1.577	2.624	7.047
	VerSe (Mode-1)	88.657	VerSe (Mode-2)	91.071	97.141	0.595	1.526	6.032
MyoPS++ (T2)	nnUNet	71.396	RITM	75.843	91.496	3.494	6.797	18.775
	TranUNet	71.499	iSegformer	52.826	90.717	5.076	8.886	19.038
	UTNet	70.251	SimpleClick	79.231	90.391	2.582	6.253	19.481
	SwinUNet	53.753	SegNext	72.492	91.262	4.101	7.873	19.342
	Medformer	63.140	VerSe (Mode-3)	74.096	94.183	5.557	7.772	12.506
	VerSe (Mode-1)	70.103	VerSe (Mode-2)	74.594	93.131	6.253	8.241	12.683
MyoPS++ (LGE)	nnUNet	44.412	RITM	60.234	86.735	7.694	14.531	19.878
	TranUNet	55.548	iSegformer	38.602	85.691	12.184	18.306	20.000
	UTNet	42.436	SimpleClick	65.232	84.773	8.010	13.541	20.000
	SwinUNet	41.365	SegNext	61.153	86.879	9.194	15.367	19.643
	Medformer	36.821	VerSe (Mode-3)	66.293	95.024	6.275	8.735	13.939
	VerSe (Mode-1)	57.879	VerSe (Mode-2)	65.238	94.752	6.867	9.531	14.235
LAScarQS++ (LGE)	nnUNet	84.827	RITM	82.957	92.704	3.550	6.163	13.866
	TranUNet	83.441	iSegformer	72.017	92.750	4.527	7.546	14.896
	UTNet	85.275	SimpleClick	84.056	91.279	3.724	6.433	14.908
	SwinUNet	79.786	SegNext	84.284	94.011	2.558	4.673	10.961
	Medformer	82.378	VerSe (Mode-3)	85.841	97.452	2.103	2.940	5.717
	VerSe (Mode-1)	83.159	VerSe (Mode-2)	86.919	97.172	1.414	2.270	5.077

VerSe (Mode-3) consistently achieves the best Dice scores and lower interaction costs among six out of seven datasets. Notably, on larger datasets, such as ACDC, M&Ms, and LAScarQS++, VerSe achieves the best performance across all metrics, significantly outperforming existing methods. For example, on the M&Ms dataset, which has the largest number of instances, VerSe achieves a Dice(1) score of 89.757%, significantly surpassing SimpleClick (85.335%) and SegNext (85.197%). This demonstrates VerSe’s ability to handle complex and large-scale data efficiently. Furthermore, as illustrated in Fig. 4, VerSe not only achieves faster convergence but also demonstrates steady improvements in segmentation accuracy as the number of clicks increases, highlighting the efficiency of its interactive prompting mechanism.

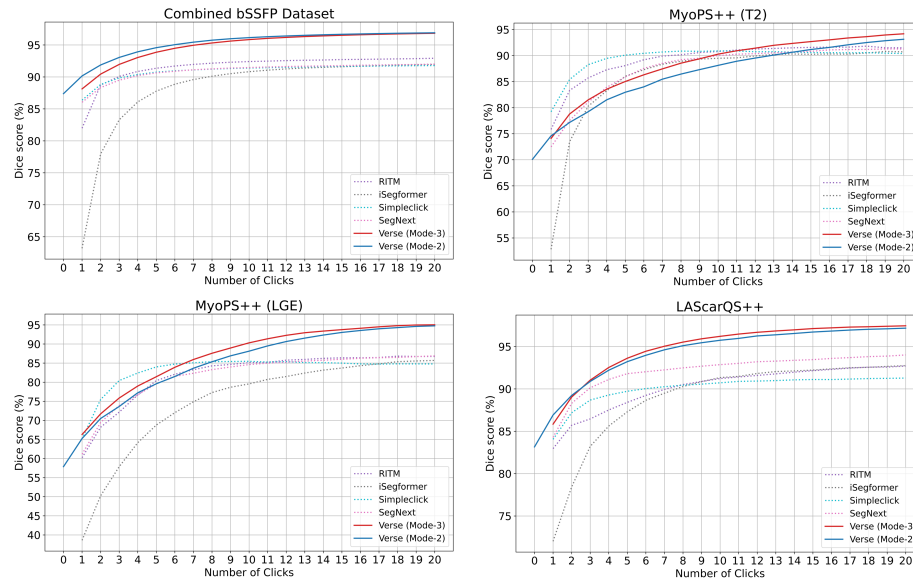


Fig. 4. Convergence analysis for models tested on four types of segmentation targets. The Combined bSSFP Dataset, including ACDC, M&Ms, M&Ms-2, and MyoPS++ (bSSFP), focuses on LV, Myo, and RV structures. **VerSe** demonstrates consistent accuracy improvements across all tasks as the number of clicks increases.

On smaller and more challenging datasets, such as MyoPS++ (LGE) and MyoPS++ (T2), **VerSe** continues to show significant advantages. On the MyoPS++ (LGE) dataset, **VerSe** achieves a Dice(20) of 95.024%, far exceeding the $\sim 85\%$ average of competing methods. Similarly, on the MyoPS++ (T2) dataset, while SimpleClick initially leads in the first 10 clicks, **VerSe** demonstrates more sustained improvements, ultimately achieving the best Dice(20) of 94.183% and a NoC95 of 12.506. These results highlight **VerSe**'s ability to efficiently utilize user interactions to refine segmentation results, even in difficult scenarios.

Overall, **VerSe** (Mode-3) sets a new benchmark in interactive segmentation, by achieving SOTA performance with minimal interaction costs. Its robust performance across both large-scale datasets and complex segmentation tasks underscores its adaptability and effectiveness in diverse cardiac MRI applications.

VerSe (Mode-2) vs. VerSe (Mode-3). Table 2 presents a detailed comparison between **VerSe** operating in Mode-2 and Mode-3 across various datasets. **VerSe** (Mode-2) achieves superior performance in 4 out of 7 datasets compared to **VerSe** (Mode-3), particularly in the ACDC and M&Ms datasets, where the initial automatic segmentation effectively reduces user interaction while improving accuracy. In contrast, **VerSe** (Mode-3), which relies solely on interactive segmentation without automatic initialization, excels on datasets where precise

automatic initialization is particularly challenging, such as MyoPS++ (T2) and MyoPS++ (LGE). These results underscore the robust interactive segmentation performance of **VerSe** (Mode-3), especially in scenarios lacking reliable automatic initialization. Meanwhile, Mode-2’s dependence on object queries highlights the need for larger and more diverse datasets to unlock its full potential. For datasets with limited training samples, Mode-3 serves as a reliable fallback. These results highlight the flexibility and adaptability of **VerSe**’s unified segmentation framework in addressing varying clinical and data-specific needs.

Out-of-Distribution Evaluation. We trained all interactive segmentation models using cardiac MRI datasets, while we evaluated their performance on out-of-distribution datasets. The results are summarized in Table 3. On the BraTS dataset, **VerSe** achieves a remarkable Dice score of 94.492% with just 10 clicks, significantly outperforming other models. In addition, it delivers the highest Dice(20) score of 96.811% and demonstrates the best annotation efficiency. On the OAI ZIB dataset, **VerSe** achieves the lowest NoC80 value of 11.787, highlighting its superior efficiency. These results collectively showcase the robust generalization capabilities of **VerSe** across diverse medical imaging domains.

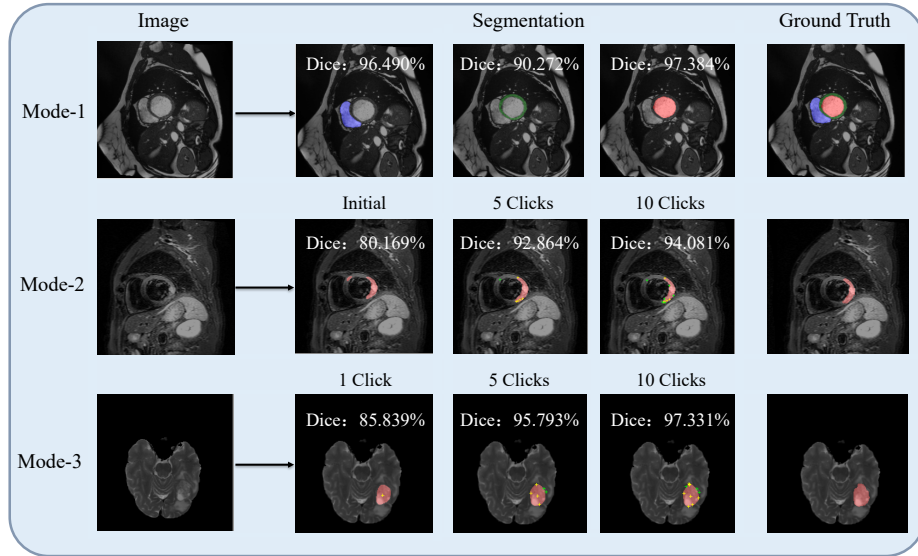


Fig. 5. Segmentation results of **VerSe** on different medical image segmentation tasks. First row: Automatic segmentation of three structures on cardiac cine MRI. Second row: Interactive refinement of myocardial edema segmentation on cardiac T2-weighted MRI. Third row: Interactive segmentation of a tumor on out-of-distribution brain MRI.

Table 3. Out-of-distribution evaluation on BraTS [2] and OAIZIB [1] datasets. **VerSe** shows strong generalizability in its interactive segmentation.

Model	OAIZIB			BraTS		
	Dice(10) \uparrow	Dice(20) \uparrow	NoC80 \downarrow	Dice(10) \uparrow	Dice(20) \uparrow	NoC80 \downarrow
RITM	70.334	79.071	13.988	88.925	93.898	5.136
iSegformer	65.509	76.784	17.063	86.465	92.281	6.482
SimpleClick	73.260	82.523	12.976	92.537	93.927	3.436
SegNext	57.211	76.261	17.427	77.448	91.619	9.604
VerSe (Mode-3)	69.516	80.631	11.787	94.492	96.811	2.777

Visualization. In Fig. 5, we demonstrate representative segmentation results of **VerSe** on cardiac MRI and out-of-distribution brain MRI. As can be seen from the results, our design of **VerSe** allows it to handle different medical image segmentation tasks with high versatility.

Table 4. Ablation study of each model component in **VerSe** under working Mode-3. ‘S’: Semantic feature queries. ‘F-B’: Foreground-background masked attention of click queries. ‘R’: Residual connection.

Model	S	F-B	R	Dice(1) \uparrow	Dice(20) \uparrow	NoC90 \downarrow	NoC95 \downarrow
A1	\times	\checkmark	\checkmark	89.563	96.537	2.543	7.015
A2	\checkmark	\times	\checkmark	90.351	96.540	2.112	6.511
A3	\checkmark	\checkmark	\times	88.480	96.172	2.755	7.513
VerSe	\checkmark	\checkmark	\checkmark	91.025	96.659	2.028	6.372

3.2 Ablation Studies

In this section, we conducted ablation studies to demonstrate the effectiveness of our model design. All of our ablation studies were conducted on the ACDC dataset with **VerSe** working in Mode-3 only. The results are shown in Table 4. (1) In model A1, we eliminated the semantic feature queries \mathbf{X}_f from click queries \mathbf{X}_c . (2) In model A2, we eliminated the masked attention branch (see the rightmost hybrid attention blocks in Fig. 3(b)) of negative click queries but combined positive and negative click query masked attention branches as a single one. (3) In model A3, we eliminated the residual connections across different scales. The results show that each of the three model components are necessary for the high performance of our model.

4 Conclusion

In this work, we propose **VerSe**, a novel framework that unifies automatic and interactive segmentation modes, through a multi-query integration mechanism. By

effectively leveraging both object and click queries, **VerSe** achieves state-of-the-art performance in both segmentation accuracy and interaction efficiency. Our experiments on seven cardiac MRI datasets and two out-of-distribution medical imaging datasets demonstrate the robustness, efficiency, and generalizability of the proposed method. **VerSe** not only bridges the gap between automatic and interactive segmentation but also sets a new benchmark for versatile image segmentation tasks. Future directions include extending the framework to handle natural data, improving scalability for larger multi-modal datasets, and enhancing interpretability for clinical adoption.

References

1. Ambellan, F., Tack, A., Ehlke, M., Zachow, S.: Automated segmentation of knee bone and cartilage combining statistical shape knowledge and convolutional neural networks: Data from the osteoarthritis initiative. *Medical image analysis* **52**, 109–118 (2019)
2. Baid, U., Ghodasara, S., Mohan, S., Bilello, M., Calabrese, E., Colak, E., Farahani, K., Kalpathy-Cramer, J., Kitamura, F.C., Pati, S., et al.: The rsna-asnr-miccai brats 2021 benchmark on brain tumor segmentation and radiogenomic classification. *arXiv preprint arXiv:2107.02314* (2021)
3. Bernard, O., Lalande, A., Zotti, C., Cervenansky, F., Yang, X., Heng, P.A., Cetin, I., Lekadir, K., Camara, O., Ballester, M.A.G., et al.: Deep learning techniques for automatic mri cardiac multi-structures segmentation and diagnosis: is the problem solved? *IEEE transactions on medical imaging* **37**(11), 2514–2525 (2018)
4. Bernard, O., Lalande, A., Zotti, C., Cervenansky, F., Yang, X., Heng, P.A., Cetin, I., Lekadir, K., Camara, O., Ballester, M.A.G., et al.: Deep learning techniques for automatic mri cardiac multi-structures segmentation and diagnosis: is the problem solved? *IEEE transactions on medical imaging* **37**(11), 2514–2525 (2018)
5. Campello, V.M., Gkontra, P., Izquierdo, C., Martin-Isla, C., Sojoudi, A., Full, P.M., Maier-Hein, K., Zhang, Y., He, Z., Ma, J., et al.: Multi-centre, multi-vendor and multi-disease cardiac segmentation: the m&ms challenge. *IEEE Transactions on Medical Imaging* **40**(12), 3543–3554 (2021)
6. Cao, H., Wang, Y., Chen, J., Jiang, D., Zhang, X., Tian, Q., Wang, M.: Swin-unet: Unet-like pure transformer for medical image segmentation. In: *European conference on computer vision*. pp. 205–218. Springer (2022)
7. Carion, N., Massa, F., Synnaeve, G., Usunier, N., Kirillov, A., Zagoruyko, S.: End-to-end object detection with transformers. In: *European conference on computer vision*. pp. 213–229. Springer (2020)
8. Chen, J., Lu, Y., Yu, Q., Luo, X., Adeli, E., Wang, Y., Lu, L., Yuille, A.L., Zhou, Y.: Transunet: Transformers make strong encoders for medical image segmentation. *arXiv preprint arXiv:2102.04306* (2021)
9. Cheng, B., Misra, I., Schwing, A.G., Kirillov, A., Girdhar, R.: Masked-attention mask transformer for universal image segmentation. In: *Proceedings of the IEEE/CVF conference on computer vision and pattern recognition*. pp. 1290–1299 (2022)
10. Cheng, H.K., Oh, S.W., Price, B., Lee, J.Y., Schwing, A.: Putting the object back into video object segmentation. In: *Proceedings of the IEEE/CVF Conference on Computer Vision and Pattern Recognition*. pp. 3151–3161 (2024)

11. Ding, W., Li, L., Qiu, J., Wang, S., Huang, L., Chen, Y., Yang, S., Zhuang, X.: Aligning multi-sequence cmr towards fully automated myocardial pathology segmentation. *IEEE Transactions on Medical Imaging* (2023)
12. Ding, Y., Li, L., Wang, W., Yang, Y.: Clustering propagation for universal medical image segmentation. In: *Proceedings of the IEEE/CVF Conference on Computer Vision and Pattern Recognition*. pp. 3357–3369 (2024)
13. Dosovitskiy, A.: An image is worth 16x16 words: Transformers for image recognition at scale. *arXiv preprint arXiv:2010.11929* (2020)
14. Gao, Y.: Training like a medical resident: Context-prior learning toward universal medical image segmentation. In: *Proceedings of the IEEE/CVF Conference on Computer Vision and Pattern Recognition*. pp. 11194–11204 (2024)
15. Gao, Y., Zhou, M., Liu, D., Yan, Z., Zhang, S., Metaxas, D.N.: A data-scalable transformer for medical image segmentation: architecture, model efficiency, and benchmark. *arXiv preprint arXiv:2203.00131* (2022)
16. Gao, Y., Zhou, M., Metaxas, D.N.: Utnet: a hybrid transformer architecture for medical image segmentation. In: *Medical Image Computing and Computer Assisted Intervention–MICCAI 2021: 24th International Conference, Strasbourg, France, September 27–October 1, 2021, Proceedings, Part III 24*. pp. 61–71. Springer (2021)
17. He, K., Zhang, X., Ren, S., Sun, J.: Deep residual learning for image recognition. In: *Proceedings of the IEEE conference on computer vision and pattern recognition*. pp. 770–778 (2016)
18. Isensee, F., Jaeger, P.F., Kohl, S.A., Petersen, J., Maier-Hein, K.H.: nnu-net: a self-configuring method for deep learning-based biomedical image segmentation. *Nature methods* **18**(2), 203–211 (2021)
19. Kirillov, A., Mintun, E., Ravi, N., Mao, H., Rolland, C., Gustafson, L., Xiao, T., Whitehead, S., Berg, A.C., Lo, W.Y., et al.: Segment anything. In: *Proceedings of the IEEE/CVF International Conference on Computer Vision*. pp. 4015–4026 (2023)
20. Li, L., Wu, F., Wang, S., Luo, X., Martín-Isla, C., Zhai, S., Zhang, J., Liu, Y., Zhang, Z., Ankenbrand, M.J., et al.: Myops: A benchmark of myocardial pathology segmentation combining three-sequence cardiac magnetic resonance images. *Medical Image Analysis* **87**, 102808 (2023)
21. Li, L., Wu, F., Yang, G., Xu, L., Wong, T., Mohiaddin, R., Firmin, D., Keegan, J., Zhuang, X.: Atrial scar quantification via multi-scale cnn in the graph-cuts framework. *Medical image analysis* **60**, 101595 (2020)
22. Li, L., Zimmer, V.A., Schnabel, J.A., Zhuang, X.: Atrialgeneral: domain generalization for left atrial segmentation of multi-center lge mris. In: *Medical Image Computing and Computer Assisted Intervention–MICCAI 2021: 24th International Conference, Strasbourg, France, September 27–October 1, 2021, Proceedings, Part VI 24*. pp. 557–566. Springer (2021)
23. Li, L., Zimmer, V.A., Schnabel, J.A., Zhuang, X.: Atrialjsqnet: a new framework for joint segmentation and quantification of left atrium and scars incorporating spatial and shape information. *Medical image analysis* **76**, 102303 (2022)
24. Li, L., Zimmer, V.A., Schnabel, J.A., Zhuang, X.: Medical image analysis on left atrial lge mri for atrial fibrillation studies: A review. *Medical image analysis* **77**, 102360 (2022)
25. Lin, J., Chen, J., Yang, K., Roitberg, A., Li, S., Li, Z., Li, S.: Adaptiveclick: Click-aware transformer with adaptive focal loss for interactive image segmentation. *IEEE Transactions on Neural Networks and Learning Systems* pp. 1–15 (2024). <https://doi.org/10.1109/TNNLS.2024.3378295>

26. Liu, J., Zhang, Y., Chen, J.N., Xiao, J., Lu, Y., A Landman, B., Yuan, Y., Yuille, A., Tang, Y., Zhou, Z.: Clip-driven universal model for organ segmentation and tumor detection. In: Proceedings of the IEEE/CVF International Conference on Computer Vision. pp. 21152–21164 (2023)
27. Liu, Q., Cho, J., Bansal, M., Niethammer, M.: Rethinking interactive image segmentation with low latency high quality and diverse prompts. In: Proceedings of the IEEE/CVF Conference on Computer Vision and Pattern Recognition. pp. 3773–3782 (2024)
28. Liu, Q., Xu, Z., Bertasius, G., Niethammer, M.: Simpleclick: Interactive image segmentation with simple vision transformers. In: Proceedings of the IEEE/CVF International Conference on Computer Vision. pp. 22290–22300 (2023)
29. Liu, Q., Xu, Z., Jiao, Y., Niethammer, M.: isegformer: interactive segmentation via transformers with application to 3d knee mr images. In: International Conference on Medical Image Computing and Computer-Assisted Intervention. pp. 464–474. Springer (2022)
30. Milletari, F., Navab, N., Ahmadi, S.A.: V-net: Fully convolutional neural networks for volumetric medical image segmentation. In: 2016 fourth international conference on 3D vision (3DV). pp. 565–571. Ieee (2016)
31. Pennell, D.J., Mohiaddin, R.H.: Cardiovascular magnetic resonance: Past, present, and future. *Circulation: Cardiovascular Imaging* **17**(8), e016523 (2024)
32. Qiu, J., Li, L., Wang, S., Zhang, K., Chen, Y., Yang, S., Zhuang, X.: Myops-net: Myocardial pathology segmentation with flexible combination of multi-sequence cmr images. *Medical image analysis* **84**, 102694 (2023)
33. Romero R, W.A., Viallon, M., Spaltenstein, J., Petrusca, L., Bernard, O., Belle, L., Clarysse, P., Croisille, P.: Cmrsegtools: An open-source software enabling reproducible research in segmentation of acute myocardial infarct in cmr images. *Plos one* **17**(9), e0274491 (2022)
34. Ronneberger, O., Fischer, P., Brox, T.: U-net: Convolutional networks for biomedical image segmentation. In: Medical image computing and computer-assisted intervention–MICCAI 2015: 18th international conference, Munich, Germany, October 5–9, 2015, proceedings, part III 18. pp. 234–241. Springer (2015)
35. Sofiiuk, K., Petrov, I.A., Konushin, A.: Reviving iterative training with mask guidance for interactive segmentation. In: 2022 IEEE International Conference on Image Processing (ICIP). pp. 3141–3145. IEEE (2022)
36. Xu, N., Price, B., Cohen, S., Yang, J., Huang, T.S.: Deep interactive object selection. In: Proceedings of the IEEE conference on computer vision and pattern recognition. pp. 373–381 (2016)
37. Yan, K., Yin, X., Xia, Y., Wang, F., Wang, S., Gao, Y., Yao, J., Li, C., Bai, X., Zhou, J., et al.: Liver tumor screening and diagnosis in ct with pixel-lesion-patient network. In: International Conference on Medical Image Computing and Computer-Assisted Intervention. pp. 72–82. Springer (2023)
38. Zhou, H.Y., Guo, J., Zhang, Y., Han, X., Yu, L., Wang, L., Yu, Y.: nnformer: Volumetric medical image segmentation via a 3d transformer. *IEEE Transactions on Image Processing* (2023)
39. Zhuang, X.: Multivariate mixture model for myocardial segmentation combining multi-source images. *IEEE transactions on pattern analysis and machine intelligence* **41**(12), 2933–2946 (2019)